Atmos. Chem. Phys. Discuss., 11, 4447–4485, 2011
www.atmos-chem-phys-discuss.net/11/4447/2011/
doi:10.5194/acpd-11-4447-2011

Atmospheric Chemistry and Physics Discussions

Correlation of black carbon aerosol and carbon monoxide concentrations measured in the high-altitude environment of Mt. Huangshan, Eastern China

X. L. Pan[1,2], Y. Kanaya[1], Z. F. Wang[2], Y. Liu[3], P. Pochanart[1], H. Akimoto[1], H. B. Dong[2], and J. Li[2]

[1]Research Institute for Global Change, Japan Agency for Marine-Earth Science and Technology, Japan
[2]State Key Laboratory of Atmospheric Boundary Layer Physics and Atmospheric Chemistry (LAPC), Institute of Atmospheric Physics, Chinese Academy of Sciences, Beijing, China
[3]Institutes of Atmospheric Physics, Chinese Academy of Sciences, Beijing, China

Received: 6 January 2011 – Accepted: 21 January 2011 – Published: 8 February 2011

Correspondence to: X. L. Pan (xlpanelf@gmail.com)

Published by Copernicus Publications on behalf of the European Geosciences Union.

Abstract

Understanding the relationship between black carbon (BC) and carbon monoxide (CO) will help improve BC emission inventories and the evaluation of global/regional climate forcing effects. In the present work, the BC (PM_1) and CO mixing ratio was continuously measured at a high-altitude background station on the summit of Mt Huangshan between 2006 and 2009. Annual mean BC concentration was $654.6 \pm 633.4\,ng\,m^{-3}$ with maxima in spring and autumn, when biomass was burned over a large area in Eastern China. The yearly averaged CO concentration was 446.4 ± 167.6 ppbv, and the increase in the CO concentration was greatest in the cold season, implying that the large-scale domestic coal/biofuel combustion for heating has an effect. The BC–CO relationship was found to have different seasonal features but strong positive correlation ($R > 0.8$). Back trajectory cluster analysis showed that the ΔBC/ΔCO ratio of plumes from the Yangtze River Delta region was $6.58 \pm 0.96\,ng\,m^{-3}\,ppbv^{-1}$, which is consistent with result from INTEX-B emission inventory. The ΔBC/ΔCO ratios for air masses from Northern, Central Eastern and Southern China were 5.2 ± 0.63, 5.65 ± 0.58 and $5.21 \pm 0.93\,ng\,m^{-3}\,ppbv^{-1}$, respectively. Over the whole observation period, the ΔBC/ΔCO ratio had unimodal diurnal variations and had a maximum during the day (09:00–17:00 LST) and minimum at night (21:00–04:00 LST) in spring, summer, autumn and winter, indicating the effects of the intrusion of clean air mass from the high troposphere. The case study combined with measurements of urban PM_{10} concentrations and satellite observations demonstrated that the ΔBC/ΔCO ratio for a plume of burning biomass was $12.4\,ng\,m^{-3}\,ppbv^{-1}$ and that for urban plumes in Eastern China was $5.3 \pm 0.53\,ng\,m^{-3}\,ppbv^{-1}$. Transportation and industry were deemed as controlling factors of the BC–CO relationship and major contributions to atmospheric BC and CO loadings in urban areas. The loss of BC during transportation was also investigated on the basis of the ΔBC/ΔCO–RH relationship along air mass pathways, and the results showed that 30–50% BC was lost when air mass traveled under higher RH conditions (>60%) for 2 days.

ACPD
11, 4447–4485, 2011

1 Introduction

Black carbon (BC) is an important component of atmospheric aerosols and a short-lived climate forcing agent, and it is mostly related to the incomplete combustion of fossil fuels and bio-fuels used for energy (Bond et al., 2004). Industrial and residential mobile resources as well as biomass burning account for the majority of emissions. Suspended BC could disturb the vertical temperature distribution in the atmosphere by absorbing more incoming and reflected radiation (Babu et al., 2002; Chung and Seinfeld, 2005; Badarinath and Latha, 2006), and it also serves as condensation nuclei and thus alters cloud properties (e.g., color, formation, life span, and albedo) and affects the level of radiation reaching the surface (Conant et al., 2002; Nenes et al., 2002; Cozic et al., 2008; Kuwata et al., 2009; Liu et al., 2009). Anthropogenic fine-mode BC particles increase the regional atmospheric opacity (Seinfeld, 2008) and have detrimental health effects (Oberdörster and Yu, 1990; Ramanathan, 2007). Severe environmental problems such as the acceleration of glacier melting have been found to be associated with BC sedimentation (Ming et al., 2008, 2009; Ramanathan and Carmichael, 2008; Thevenon et al., 2009).

Our understanding of the role that BC plays in climate change has been revised dramatically over the past decade. In the Intergovernmental Panel on Climate Change (IPCC) Third Assessment Report (IPCC, 2001), the contribution of BC (mainly from the burning of fossil fuel and biomass) to climate warming was described as "very low". Chief culprits of climate warming were considered carbon dioxide (CO_2), methane (CH_4), nitrous oxide (N_2O), ozone and other greenhouse gases (GHGs) such as hydrofluorocarbons, per-fluorocarbons, and SF_6, most of which have come from the substantial emission of human activities since the pre-industrial era. Recently, observations and modeling have increasingly suggested a relatively strong positive climate forcing effect of carbonaceous aerosols. BC forcing at the top-of-atmosphere was estimated to be as much as 55% of the CO_2 forcing with a mean value of 0.9 W m^{-2} (and range from 0.4 to 1.2 W m^{-2}) (Ramanathan and Carmichael, 2008). The extent of BC-induced

ACPD
11, 4447–4485, 2011

warming is highly determined by the atmospheric loading of soot particle mass concentrations (Sato et al., 2003), sulphate and organic coatings (Ramana et al., 2010), their shapes (Adachi et al., 2010) and mixing state (Jacobson, 2001; Schwarz et al., 2008; Naoe et al., 2009).

Significant emissions of pollutants (e.g., BC and CO) in East Asia due to ever-quickening industrial development, surging automobile ownership, and intensive seasonal burning of biomass are well known (Streets et al., 2001; Bond et al., 2004; Streets and Aunan, 2005; Zhang et al., 2009). Bottom-up statistical methods, widely used to investigate regional emission inventories (Streets et al., 2001; Cao et al., 2006; Ohara et al., 2007), indicate that more than one-fourth of BC originates from China; however, variations in the emisstion strengths of different fuel types and combustion conditions produce large uncertainties (Bond et al., 2004), which make continuous measurements in highly polluted and remote areas important in better estimating regional characteristics and constraining the highly uncertain emission rate of BC (Kondo et al., 2006; Han et al., 2009). Observations made in 14 Chinese cites indicated that more than two-thirds of urban carbonaceous aerosols are directly emitted locally (Cao et al., 2007), and these large polluted air masses readily flow from urban areas and affect the air quality of rural areas (Uno et al., 2003; Wang et al., 2006; Li et al., 2007; Yan et al., 2008). Discrepancies in BC concentration measurements employing optical and thermal techniques have been investigated in detail at the summit of Mt Taishan (a regionally representative high-altitude site in the middle of Central Eastern China), which is frequently downwind of BC-rich polluted plumes (Kanaya et al., 2008). Meanwhile, BC has also been found to have a large effect on photochemistry-derived pollutants such as ozone (Li et al., 2005). Recently, BC to sulphate ratios determined by surface and aircraft measurements in Beijing and Shanghai indicated that fossil-fuel-dominated BC plumes have a much more efficient warming effect than biomass-burning-dominant plumes (Ramana et al., 2010).

Carbon monoxide (CO) is another product of the incomplete oxidation (Baumgardner et al., 2002). Although variations in fuel types and oxygen supply alter BC and CO

ACPD
11, 4447–4485, 2011

emissions dramatically, a remarkable correlation between BC and CO has been found in a number of studies (Jennings et al., 1996; Derwent et al., 2001; Badarinath et al., 2007; Spackman et al., 2008). Therefore, the BC–CO relationship (ΔBC/ΔCO) is deemed a good indicator both for distinguishing different pollutant sources in case studies (Kondo et al., 2006; Spackman et al., 2008; Han et al., 2009; Subramanian et al., 2010) and validating BC emission inventories for models (Derwent et al., 2001; Dickerson et al., 2002). Near the source region, the ΔBC/ΔCO ratio should not change appreciably through air mass mixing, dilution and removal processes (wet and dry deposition for BC; oxidation by the hydroxyl radical (OH) for CO), and BC takes longer to become hydrophilic for removal in conditions of relatively low humidity (Baumgardner et al., 2002).

There have been few investigations on the ΔBC/ΔCO ratio in China. In this work, we concurrently measured the BC mass concentration and CO mixing ratio at the summit of Mt Huangshan from June 2006 to May 2009. The ΔBC/ΔCO ratio and air mass back trajectories were employed to investigate high-pollution episodes and their possible BC origins. In addition, we referred to the air pollution index (API, published daily by the Ministry of Environmental Protection of the People's Republic of China at http://datacenter.mep.gov.cn/report/air_daily/air_dairy.jsp) for 85 Chinese cities in determining regional pollution events. The removal efficiency of BC under different relative humidity (RH) conditions during transportation is also discussed.

2 Experimental

2.1 Site description and meteorology

BC and CO concentrations were continuously measured at a meteorological station on the summit of Mt Huangshan (30.16° N, 118.26° E, 1840 m a.s.l., Anhui province). The site is located at the southern edge of the North China Plain, which is supposed to be a heavy polluted region owing to its intense industrial/residential activities (Li et al.,

ACPD
11, 4447–4485, 2011

2008) and open burning of biomass during harvest (Yamaji et al., 2010). Pollution emitted from the Yangtze River Delta metropolis clusters (about 200 km to the northeast) is also easily transported to the site with the prevailing northeast wind. According to the NASA INTEX-B emission inventory (Zhang et al., 2009), about 4585 Gg yr^{-1} $PM_{2.5}$, 607 Gg yr^{-1} BC and 61210 Gg yr^{-1} CO were emitted in 2006 via anthropogenic activity in the region of the North China Plain, accounting for more than 35% of total emissions in China. A map of BC and CO emissions is presented in Fig. 1b.

Other considerations in the site selection were that the region is uninhabited, the surrounding 1500 km^2 had over 80% vegetation coverage of deciduous/coniferous mixed forest and grass, and local-source pollution produced by tourists is very limited. Mt Huangshan has a subtropical monsoon climate, distinct seasons and abundant rainfall in summer (peaking in July). According to statistical analysis of 48-h air mass back trajectories (Hysplit4 version 4.9u, http://ready.arl.noaa.gov/HYSPLIT.php), about 38%, 45% and 17% of air mass are from northerly (NE–W section), southerly (W–ESE section) and easterly (ESE–NE section) directions, respectively. This obvious difference in air mass pathways allows investigation of the origins and transportation of pollutants.

2.2 Measurements and error analysis

We measured BC mass concentrations at 1 min time intervals using a multiple-angle absorption photometer (MAAP, Model 5012, Thermo Inc.). Air samples drawn from the ambient atmosphere pass through a 5 m long, 0.5 inch wide conductive tube and a PM_1 cyclone (cut-off diameter of 1 µm, URG-2000-30EHB, USA). Assuming the BC mass-equivalent diameter (MED) has a log-normal distribution in the fine mode with a peak around 200 nm (Subramanian et al., 2010), the loss of BC particles (greater than 1 µm in diameter) is estimated at less than 10% of the BC mass (Kanaya et al., 2008; Spackman et al., 2008; Kondo et al., 2009). The instrument operates by simultaneously measuring the optical attenuation and reflection of particles deposited on a glass fibrous filter from several detection angles. Here we followed the manufacture's recommendation of using a fixed σ_{ap} value of 6.6 m^2 g^{-1} at 670 nm to convert

ACPD
11, 4447–4485, 2011

the absorption coefficient to a mass concentration. Although the calculation for the present instrument (MAAP) already takes into account corrections for removing the multi-scattering effect, optical techniques are still likely to overestimate by 5–50% the BC mass concentration compared with optical-thermal techniques owing to coating effects of non-absorbing particles on soot particles (Hitzenberger et al., 2006; Slowik et al., 2007; Chow et al., 2009). The largest discrepancy has been found to be associated with contributions of organic matter or "brown carbon" (Reisinger et al., 2008). According to inter-comparison experiments performed at a high mountain site over Central Eastern China (Kanaya et al., 2008), the MAAP-measured BC mass concentration in PM_1 was approximately the same as that measured by the particle soot absorption photometer (PSAP, Radiance Research, with inlet heated at 400 °C). Nevertheless, the concentration was approximately 50% higher than that obtained using an ECOC semi-continuous analyzer (Sunset Laboratory, USA, NIOSH protocol). Here, we employed a factor of 1.4 in converting the MAAP-measured BC mass concentration to an "EC" category. Studies carried out in Tokyo (Kondo et al., 2006) showed that mass concentrations based on the NIOSH protocol were about 20% less than those based on the IMPROVE protocol, and the uncertainty in the absorbance determined using the MAAP was estimated to be 12% (Petzold et al., 2005); therefore, the overall uncertainty was about 25%.

In situ measurement of the CO mixing ratio was carried out with a commercial gas filter non-dispersive infrared CO gas analyzer (Thermo Scientific. Model 48C, USA, time resolution of 1 min) equipped with a Nafion dryer to reduce interference by water vapor in the sampled air. The zero point (baseline of the instrumental signal) was routinely checked in the first 10 min of each hour using purified air, and span calibrations were performed in the ambient environment before (May 2006) and in the middle of the field experiments (December 2007) by injecting standard span gas (1.04 parts per million by volume (ppmv), produced by Nissan-Tanaka Corp., Japan). The difference between the span and zero points demonstrates that the measured CO mixing ratio is about 46 ppbv higher than the standard value, and the ratio was adjusted by 95% afterward.

ACPD
11, 4447–4485, 2011

The instrument baseline in the observation period has a stable linear increasing trend with a drift ratio of 0.4 ppb/h; however, this influence was easily removed by zero-point-deduction operations in subsequent data procedures. Additionally, meteorological parameters (wind, RH and temperature) were acquired from the NCEP reanalysis dataset (ftp://ftp.cdc.noaa.gov/Datasets/ncep.reanalysis/surface/) with a time interval of 6 h at the site grid.

3 ΔBC/ΔCO ratios obtained from emission inventories and uncertainties

Bottom-up statistical techniques are regularly used to construct pollution emission inventories on the basis of energy consumption information (classified by province, economic sector and fuel/product type) and available experimental emission factors for different species (Streets et al., 2001; Cao et al., 2006; Zhang et al., 2009). They are widely accepted for simulations of chemical transport models. According to the NASA INTEX-B mission 2006, the mean ΔBC/ΔCO ratios of anthropogenic emissions were calculated as approximately 7.6, 6.8, 10.0, 7.9, 6.3 and 5.6 $ng\,m^{-3}\,ppbv^{-1}$ for Hebei, Shandong, Henan, Anhui, Jiangsu and Zhejiang provinces, respectively. A high value of 17.8 $ng\,m^{-3}\,ppbv^{-1}$ for Shanxi province might relate to wide-scale industrial and residential coal combustion. Owing to large urban industrial and transportation contributions, ΔBC/ΔCO was 4.1 $ng\,m^{-3}\,ppbv^{-1}$ for the Yangtze River Delta region and 3.8 $ng\,m^{-3}\,ppbv^{-1}$ for the city of Beijing. Yamaji et al. reported ΔBC/ΔCO ratios of 11.0, 11.2, 11.8, 11.4 and 11.0 $ng\,m^{-3}\,ppbv^{-1}$ for open burning of crop residue in Anhui, Hebei, Henan, Jiangsu and Shandong provinces, respectively (Yamaji et al., 2010).

The accuracy of emission inventories heavily depends on factors such as the statistical data of fuel consumption, emission factors, and the temporal/spatial allocation method. However, the necessary data are not always available owing to limited measurements and a lack of statistical investigations. For example, the amount of BC produced through residential coal usage and biofuel consumption has been identified as a major source of uncertainty (Streets et al., 2003b) owing to a lack of authorized

ACPD
11, 4447–4485, 2011

reports from government agencies and published scientific papers, and it is difficult to apply BC emission factors in estimations because there are large discrepancies in measurement results even in the same category. Previous studies (Cao et al., 2006) have reviewed the discrepancies in detail. Additionally, studies (Streets et al., 2003a; Yan et al., 2006) have shown that quantities of annually burned biomass, which are an essential quantity in BC emission estimation, did not agree well with each other, and uncertainty at the 95% confidence interval was as high as 450% (Streets et al., 2003a). The INTEX-B inventory of Zhang et al. (Zhang et al., 2009) summarized major uncertainties in anthropogenic pollutant emissions, and gave BC and CO uncertainties of 208% and 70%. Herein, the uncertainty in the ΔBC/ΔCO ratio was estimated at about 220% using the equation ($\delta = \sqrt{\delta_1^2 + \delta_2^2}$). In this case, constraining factors (such as ΔBC/ΔCO, $\Delta SO_2/\Delta CO$ and $\Delta CO/\Delta CO_2$) in a regional-scale-representative experiment are of great interest in improving the inventory.

4 BC and CO temporal variations

4.1 Seasonal variations

A dataset comprising approximately 3 years (from 2006 June 1 to 2009 May 14) of BC mass concentrations and 1.5 years (from 25 January 2007 to 25 May 2008) of CO mass concentrations is reported here. Time series of the BC ($654.6 \pm 633.4\,ng\,m^{-3}$) and CO ($424.1 \pm 159.2$ ppbv) concentrations have large variations for the entire observation period. The hourly averaged data show that atmospheric BC loading was high (over $2000\,ng\,m^{-3}$) mostly in spring and autumn, and the CO concentration was high (over 1000 ppbv) in December, January and February. Urban pollution resulting from the industrial and residential burning of biofuel for cooking and heating are the most probable explanations for such phenomena. Figure 2 illustrates monthly averaged variations in BC and CO concentrations. The CO concentration generally had a winter maximum and summer minimum, and varied greatly in winter owing to the

ACPD
11, 4447–4485, 2011

frequent shifting of air masses from the clean continent interior and heavily polluted urban plumes in the heating period (normally from November to March in Northern China). In summer, the CO concentration in the Mt Huangshan region apparently decreased owing to frequent intrusions of clean air mass from the Pacific Ocean, and this seasonal trend was confirmed by observations in Eastern China made by MOPITT (http://www.acd.ucar.edu/mopitt/). A slight reduction in the CO concentration with large variations in November might relate to the uncertainty of having a limited number of data ($N = 720$) because no obvious changes in pollutant emissions were expected for that season. Seasonal variations in the BC loading have a bimodal distribution with two enhancement periods of BC loading in May and October when there was large-scale burning of crop residues. The exacerbation of BC pollution probably resulted from the combustion of biomass. Considering the regional climatology, the increase in the BC concentration might also be related to the dynamic transport and planetary boundary layer (PBL) evolution characteristics in the transitional periods of the summer monsoon (May) and winter monsoon (October). In summer (from June to August), the BC concentration decreased to 319.5 (±225.0) ng m^{-3}, and back trajectory analysis indicated that more than 80% of air mass came from Southern China where the BC emission was relatively weak (Streets et al., 2001; Cao et al., 2006, 2009; Chen et al., 2009). Furthermore, wet removal was another controlling factor of BC declination, albeit there was summer strong thermal vertical convection and the full development of the PBL, which was favorable for uplifting surface pollutants to the high-altitude environment, in winter and spring, monthly averaged BC concentrations were quite stable with a mean value of 486.9 ng m^{-3}; the large variations (standard deviation of 372.4 ng m^{-3}) mostly resulted from meteorology (PBL stratification, turbulence and transportation) and regional pollutant emissions in surrounding regions.

4.2 Diurnal variations

Diurnal variations in BC, CO and ΔBC/ΔCO in different seasons are shown in Fig. 3. As expected, BC concentrations have unimodal distributions with maxima in the afternoon

ACPD
11, 4447–4485, 2011

(12:00–16:00 Local Standard Time (LST)) owing to the development of the PBL and pollution lifting with the valley breeze during the day; the BC concentrations were 824.8 ± 598.8, 571.7 ± 412.3, 1141.8 ± 811.7 and $793.7 \pm 856.5\,\mathrm{ng\,m^{-3}}$, respectively for spring, summer, autumn and winter. With suppression of the PBL at night, the BC concentrations at the site decreased to $682.2\,\mathrm{ng\,m^{-3}}$ on average in spring, autumn and winter and $448.9\,\mathrm{ng\,m^{-3}}$ in summer. Owing to the short duration of sunshine, the BC concentration in winter peaked earlier at approximately 15:00 LST, and decreased quickly afterward. Diurnal variations in CO have seasonal features. As shown in Fig. 3b, fluctuations in the CO concentration were weaker in winter and summer than in other seasons; the concentrations were 353.1 ± 93.5 and 485.3 ± 199.3 ppbv, respectively. The high CO concentrations in winter were mainly due to large-scale fossil fuels burning for heating in Northern China, the stable and lower CO loading in summer might be strongly related to the strong mixing of clean air masses from marine regions and urban plumes within the PBL. In autumn, the CO concentration increased obviously from 361.6 ± 170.2 ppbv in the morning (06:00 LST) to a maximum (472.9 ± 148.6 ppbv) in the afternoon (14:00 LST).

The correlation of BC–CO indicates pollution from certain source categories. For instance, plumes from the burning of biofuel (biomass and agriculture residues) are expected to have a much greater quantity of BC particles than urban plumes, which are abundant with vehicle and industry emissions (Spackman et al., 2008). In this manuscript, the $\Delta BC/\Delta CO$ ratio was derived using the equation $(BC - BC_0)/(CO - CO_0)$. BC_0 and CO_0 (baseline concentrations of BC and CO) were determined as mean values of the 1.25 percentile of data for spring, summer, autumn and winter, and the results were 69.3, 61.6, 42.1 and $50.4\,\mathrm{ng\,m^{-3}}$ for BC_0 and 109.21, 118.71, 90.81 and 116.1 ppbv for CO_0, respectively. BC_0 and CO_0 concentrations were generally lower than the measurement at a Beijing urban site, especially in autumn. This declination mainly reflected the baseline of clean air masses from the continent interior because more than 90% of air mass came directly from the Mongolian Plateau. The $\Delta BC/\Delta CO$ ratio had an approximately unimodal diurnal distribution (Fig. 3c). The

ACPD
11, 4447–4485, 2011

ΔBC/ΔCO ratios were on average 2.4, 2.1, 3.0 and 2.0 ng m^{-3} ppbv^{-1} during the day (09:00–17:00 LST) and 1.9, 1.7, 2.5 and 1.4 ng m^{-3} ppbv^{-1} at night (21:00–04:00 LST) in spring, summer, autumn and winter, respectively. The lower ΔBC/ΔCO ratio at night might relate to intrusions of clean air from the upper troposphere. Seasonally, the highest ΔBC/ΔCO ratio was in autumn owing to the burning of biomass, and winter had a lower ΔBC/ΔCO ratio with a maximum of 2.3 ng m^{-3} ppbv^{-1} (15:00 LST) and minimum of 1.4 ng m^{-3} ppbv^{-1}. An airborne single-particle soot photometer recorded a mean value of 2.89 ± 0.89 ng m^{-3} ppbv^{-1} at high altitude (2–5 km) over Mexico (Subramanian et al., 2010), similar to our results. The high ΔBC/ΔCO ratio (approximately 8 ng m^{-3} ppbv^{-1}) at the urban site in the early morning was considered to be due to increased emission from heavy vehicles (with diesel engines) (Kondo et al., 2006; Han et al., 2009). Nevertheless, these explanations are difficult to apply in our case because ΔBC/ΔCO was measured for plumes from different emission sources that were well mixed through convective movement.

5 Cluster analyses of regional BC and CO correlations

Forty-eight-hour back trajectory cluster analyses using 2007 NCEP meteorological data were performed to highlight the relationship between the ΔBC/ΔCO ratio and the origin of the air mass. Only BC data for which ambient RH was less than 50% for the entire air mass pathway were included in the calculations to eliminate the effect of local wet removal, and a criterion of 30% total spatial variations was applied to determine the number of clusters. Back trajectory air mass pathways were grouped into four mean cluster trajectories (Fig. 4a). Cluster #1 comprised air masses slowly moving from the west, Cluster #2 comprised air masses from Mongolia moving quickly across heavily polluted regions in Shanxi, Hebei, Henan and Shandong provinces; Cluster #3 mainly comprised air masses from the eastern sector that passed through densely populated urban areas of the Yangtze River Delta; and Cluster #4 comprised air masses from Southern China. In Fig. 4a, we also present the year-averaged PM_{10}

ACPD
11, 4447–4485, 2011

spatial distribution for 2007, with PM_{10} mass concentrations derived from daily API values for 85 Chinese cities using the government-published routine method as described by Qu et al. (Qu et al., 2010). The combination of back trajectory clusters and urban PM_{10} loadings along air mass pathways allows us to determine the probable origins of BC pollution.

BC–CO correlations for each cluster are shown in Fig. 4b. As expected, all have good linear relationships with high R values (0.86 for Cluster #1, 0.87 for Cluster #2, 0.98 for Cluster #3, and 0.94 for Cluster #4), which indicate common sources of BC and CO in spite of different origins of pollution plumes for different back trajectory clusters. The BC–CO relationship highly depends on sources and sinks in the context of pollution transportation. The $\Delta BC/\Delta CO$ ratio reported here is regionally representative on the basis of four considerations. (1) A dry deposition velocity of less than 1 mm/s was documented for sub-micron aerosol particles (MED of BC typically ranges 200–600 nm), suggesting a removal rate of about 10% per day (Derwent et al., 2001). In this study, the removal rate of BC particles during transportation is expected to be about 15–20% (which is discussed in Sect. 7), which is within the overall uncertainty of the MAAP instrument, (2) For BC aging processes (e.g., oxidation, condensation and coagulation in the atmosphere), which dominate solubility and thus the removal rate of BC particles, modeling studies have suggested an exponential lifetime of 40–80 h (Cooke and Wilson, 1996). Croft et al. suggested a conversion timescale of 4.9 days for altering insoluble BC to soluble/mixed BC through physical and oxidative processes (Croft et al., 2005). Here we screened data according to the criterion of RH (>50%) conditions at which aerosol hygroscopicity is very weak even when aerosols are coated by sulfate and nitrate substances (Pan et al., 2009), (3) Baumgardner et al. (2002) and Subramanian et al. (2010) suggested that ambient air dilution and dispersion should not appreciably alter the ratio of the two species near the source region despite the different thermal velocities and diffusion coefficients of BC and CO. (4) BC and CO from different emissions are well mixed during 48 h of convection, and $\Delta BC/\Delta CO$ here refers to a typical value on a regional scale instead of ratios of specific emission types.

ACPD
11, 4447–4485, 2011

Statistical results of BC and CO concentrations and BC–CO correlation are summarized in Table 1.

For the whole period, about 46% air masses back trajectories were classified into Cluster #1, BC and CO concentrations were $750.9 \pm 616.7\,\mathrm{ng\,m^{-3}}$ and 319.5 ± 94.7 ppbv, respectively, and $\Delta BC/\Delta CO$ was $5.65 \pm 0.58\,\mathrm{ng\,m^{-3}\,ppbv^{-1}}$; the values are similar to measurements in urban areas (Kondo et al., 2006; Spackman et al., 2008; Han et al., 2009). Simple footprint analysis (supplementary Fig. 2) indicated that urban plumes in Southern Anhui province mostly resulted in relatively high BC and CO concentrations, and domestic and industrial emissions were the major contributions. Cluster #2 consisted of 19% of total air masses back trajectories, and the $\Delta BC/\Delta CO$ ratio was relatively lower ($5.2 \pm 0.63\,\mathrm{ng\,m^{-3}\,ppbv^{-1}}$), the mean CO concentration was 356.3 ± 113.1 ppbv, and the intercept of the BC–CO correlation was 195.2 ± 24.3 ppbv (denoting the background level of CO); these values reveal that industrial emissions to the northwest, coal processing and related manufacturing in Southern Shanxi province partially contribute to high pollution loadings. Note that air masses in Cluster #2 mostly originated from above 2 km altitude; therefore, the statistical results here primarily describe the pollution conditions in the middle tropospheric environment over industrial regions. However, our results were higher than airborne measurements by Single Particle Soot Photometer in the altitude range of 2.7–4.1 km around Mexico City with a mean $\Delta BC/\Delta CO$ ratio of $2.80\,\mathrm{ng\,m^{-3}\,ppbv^{-1}}$ for fresh emissions and $3.3\,\mathrm{ng\,m^{-3}\,ppbv^{-1}}$ for 1-day-old emissions (Subramanian et al., 2010).

Cluster #3, accounting for 16% of total trajectories, comprised air masses from eastern metropolitan areas of the Yangtze River Delta (Fig. 4a). BC and CO concentrations from this sector were lower than concentrations from other origins and had means of 422.4 ng/m^3 and 244.9 ppbv, comparable to values reported for regionally polluted areas in Europe (Derwent et al., 2001). Spatial and inter-annual studies on surface PM_{10} over China have also indicated relatively low occurrences of heavy PM pollution in this area ($98.9 \pm 47.6\,\mu\mathrm{g\,m^{-3}}$) (Qu et al., 2010). However, the higher $\Delta BC/\Delta CO$ ratio ($6.58 \pm 0.96\,\mathrm{ng\,m^{-3}\,ppbv^{-1}}$) might result from significant contributions of carbonaceous

ACPD
11, 4447–4485, 2011

matter from domestic, transportation and industry sources. Studies of urban Beijing indicated motor vehicle sources accounted for 80% and 68% of carbonaceous matter during the day and at night, respectively (Zhang et al., 2007), which might be applicable to cases for the region of the Yangtze River Delta.

In Cluster #4, air masses arriving at the study site have statistically the highest BC and CO concentrations of $942.4 \pm 612.8\,\mathrm{ng\,m^{-3}}$ and 366.4 ± 111.8 ppbv, respectively. Footprint analysis demonstrates that pollution emission from Northern Jiangxi and Western Hunan provinces substantially contributed to BC and CO concentrations, and urban plumes from the region of the Pearl River Delta might also have a slight influence. For Cluster #4, the $\Delta BC/\Delta CO$ ratio had a mean of $5.21 \pm 0.93\,\mathrm{ng\,m^{-3}\,ppbv^{-1}}$ owing to the mixing and advection of air masses with different sources plumes below 1.5 km altitude. Note that all air mass back trajectories in Cluster #4 in the direction of Southern China were for November, when there was widespread indoor and outdoor burning of agricultural residues for heating in Southern China. This suggests underlying effects of the burning of biomass, which was confirmed through remote sensing by MODIS (http://firefly.geog.umd.edu/firemap/). Additionally, the high value of the BC–CO correlation intercept (186.8 ± 38.7 ppbv) suggests strong CO emissions over that region; nevertheless, there are few large cities (with populations over 1 million, http://www.gov.cn, as shown in Fig. 4a) in that region, suggesting possible CO sources in rural or less-developed regions instead of contributions from urban and industrial emissions.

6 Characteristics in cases of heavy BC pollution

There were six episodes of heavy BC pollution at the observation site, with the average BC concentration being $1661.2\,\mathrm{ng\,m^{-3}}$. Here daily averaged BC concentrations over $1000\,\mathrm{ng\,m^{-3}}$ and RH less than 50% were taken as the criterion of high BC pollution. Table 2 summarizes each episode. As expected, heavy BC pollution was accompanied by high CO concentrations with a mean value of 509.1 ppbv. According to air mass

ACPD
11, 4447–4485, 2011

back trajectories, the observation site was occasionally located downwind of different types of sources. Combining analysis with hotspots detected by MODIS and the urban PM_{10} mass concentration distribution (Figs. 6 and 7), we divided the six episodes into two categories (Table 2). On 29–31 January, 6 February, and 28 and 29 October 2007 (labeled episodes 1, 2, 3, 4, respectively in Fig. 5), the site was mainly affected by urban plumes, while open burning played a dominant role on 22–24 October and 6–8 January 2008 (labeled episodes 5 and 6 in Fig. 5; hotspots are shown in supplementary Fig. 3). Statistical information of the BC and CO correlation is summarized in Table 2.

6.1 Urban plumes

As shown in Table 2, the range of variation in ΔBC/ΔCO for urban plumes was 5.0–5.8 $ng\,m^{-3}\,ppbv^{-1}$, and ΔBC/ΔCO ratios for different urban plume episodes were in general agreement in spite of large variations in CO concentrations. For instance, the daily mean CO concentration on 29 October was 743.8 ppbv, more than twice that on 28 October, while the ΔBC/ΔCO ratio varied by only 15%. The consistency of the ΔBC/ΔCO ratio suggests common sources of BC and CO emissions. Experiments performed at urban sites have shown that vehicle exhaust is the most important source of BC and CO, and their concentration ratio highly depends on the fractions of heavy diesel vehicles and light gasoline vehicles (Kondo et al., 2006; Han et al., 2009). Back trajectory analysis showed that all air masses passed through heavily polluted areas before arriving at the study site; therefore, urban transportation emissions could partially explain the ΔBC/ΔCO accordance. However, we cannot exclude the influences of industrial or residential emissions because of the lack of evidence from specific tracer measurements. On 29–31 January 2007 (episode 1), air masses mostly originated from the northwest, and they quickly travelled more than 1000 km, which implies significant influence close by such as in Henan and Hubei provinces because of the strong dilution of plumes with long transportation times. For example, Wuhan (west of the observation site at 30.6° N, 114.3° E) experienced heavy pollution with daily averaged PM_{10} mass concentrations of 236 and 212 $\mu g\,m^{-3}$ on 29 January and 31 January 2007,

ACPD
11, 4447–4485, 2011

respectively. On 6 February 2007 (episode 2), urban plumes arrived from Southern China, and the daily BC mass concentration was the highest with a mean of 1797.5 ng m^{-3}. The enhancement was mostly related to residential emissions from less-developed small towns. Air masses were mainly stagnant in Hubei province on 28 October (episode 3), and the ΔBC/ΔCO ratio increased to 5.8 ng m^{-3} ppbv^{-1}; however, this value was still lower than the quantitative result (Supplement Fig. 8) obtained from the emission inventory. During episode 4, a high background level of CO concentrations (527.7 ppbv, intercept of linear regression) illustrated that CO build-up might be due to other emissions under stable meteorological conditions, and industrial and domestic sources in downstream areas of the Yangtze River are the most likely according to back trajectories (Fig. 6d). The emission inventory of INTEX-B also suggests strong emissions of CO in Jiangsu province. We believe BC and CO were well mixed and had constant ΔBC/ΔCO ratios soon after emission in certain areas, notwithstanding variations in emission strengths for different industry types.

6.2 Biomass burning

The ΔBC/ΔCO values was 12.4 ± 1.5 ng m^{-3} ppbv^{-1} during biomass burning influencing periods. There were two episodes of strong influences of burning biomass (22–24 October 2007, and 6–8 January 2008) in the observation period according to satellite remote sensing. On 22–24 October, air masses were nearly stagnant south of the observation site (Fig. 7), and more than 35 hotspots were confidently detected by the MODIS satellite. CALIPSO satellite results also indicated heavy "smoke" plumes at a 2–3 km altitude distributed over 25° N–30° N in Southern China (shown in supplementary Fig. 6). On 6–8 January 2008 (episode 6), more than 800 hotspots in surrounding regions were detected by MODIS, and more than 60 cities exceeded the class 2 limit value (150 μg m^{-3} daily) of the National Ambient Air Quality Standard. Daily PM_{10} mass concentrations in urban areas along the air mass back trajectories were 182.2 μg m^{-3} (on 6 January) and 220.0 μg m^{-3} (on 8 January). According to vertical profile information provided by CALIPSO observations, the pollution in the

ACPD
11, 4447–4485, 2011

25° N–32° N latitude range was related to "smoke" and "polluted continental" plumes (shown in supplementary Fig. 7), and the aerosol optical depth at 550 nm observed by MODIS in this region exceeded 0.9 (http://gdata1.sci.gsfc.nasa.gov/daac-bin/G3/gui.cgi?instance_id=MODIS_DAILY_L3). We thus assumed that this episode involved the mixing of aerosol from biomass burning and urban plumes.

As a result of the open burning of biomass, BC mass concentrations significantly increased to 2452.2 and 2294.7 ng m^{-3} in these two episodes, respectively. On 22–24 October 2007, the maximum BC concentration even exceeded 5000 ng m^{-3}, which was about 4 times that in episodes of urban pollution, and the mean ΔBC/ΔCO reached 12.4 ng m^{-3} $ppbv^{-1}$, which is comparable to results reported for Texas that ΔBC/ΔCO exceeded 9 ng/kg/ppbv (equal to 11.1 ng m^{-3} $ppbv^{-1}$ assuming air density of 1.25 kg m^{-3}) in biomass burning plumes (Spackman et al., 2008). Observations in India indicated strong BC emissions, with a ΔBC/ΔCO ratio of 28.5 (μg m^{-3})/(μg m^{-3}) during the forest fire season (Badarinath et al., 2007). According to the emission inventory, BC emission factors for biomass burning were about 0.47–0.98 g kg^{-1} owing to incomplete combustion and much higher than those for urban gasoline vehicle emissions. Episode 6 (6–8 January 2008) was also affected by urban plumes according to comprehensive analysis, and the ΔBC/ΔCO ratio decreased to 7.5 ± 0.18 ng m^{-3} $ppbv^{-1}$.

7 Estimation of BC loss

As mentioned above, major uncertainty of ΔBC/ΔCO ratio came from the dry deposition of BC particles (they collided or absorbed with other hydrophilic substances, gradually grew larger in the higher RH environment, and subsequently were removed from atmosphere according to gravitational settling and turbulence transportation), and atmospheric BC concentration was also affected by rain-out processes (not addressed here). Figure 8 shows the dependence of the ΔBC/ΔCO ratio on RH in the absent of rain along transportation path. For better expression, RH was divided into six ranges (RH > 80%, 85% > RH > 65%, 75% > RH > 55%, 65% > RH > 45%, 55% > RH > 35%

ACPD
11, 4447–4485, 2011

and RH < 40%), and only BC data that met the required RH criterion for the entire air mass pathway were used in calculations. Statistical results for all non-rain periods and each cluster are summarized in Table 3. The table shows that over 90% of BC was lost when pollution air masses remained for more than 48 h in an environment with RH exceeding 80%. In summer, air masses from Southern China mostly had high RH (over 70% on average), which suggested more than 60% of BC became hygroscopic as a result of coagulation and aging processes and was lost during the two day transportation. In Fig. 8, it is noteworthy that the loss rate at higher RH (over 80%) of air masses from Southeastern China (blue crosses) was about three times that of air masses from Northern China (green crosses). This phenomenon is mostly attributed to differences in the chemical compositions and size distribution of aerosol particles. The abundance of crustal materials typically associated with dust led to the aerosol from Northern China being less hygroscopic, while anthropogenic fine-mode particles were a major contribution to aerosol mass concentrations in Southern China. Water-soluble inorganic salts (e.g., sulfate and nitrate) and organic carbon matter (normally hydrophobic) and their mixing states also affected the capacity of BC to absorb water. According to the INTEX-B anthropogenic emission inventory, the proportion of organic matter in the $PM_{2.5}$ category from Northern China (in Cluster #2) was about twice that of the Yangtze River Delta region (Supplementary Fig. 8), and primary organic aerosols account for more than 60% of total organic matter (Han et al., 2008). These features might be another reason for a lower loss rate.

8 Comparison with other studies and discussions

Significant differences in the ΔBC/ΔCO ratio for fumes of burning biomass and urban plumes have been documented by many previous studies. In the present work, the ΔBC/ΔCO ratio was $12.4 \pm 1.5\,\mathrm{ng\,m^{-3}\,ppbv^{-1}}$ for an episode of burning biomass and comparable to the measurements for Texas (Spackman et al., 2008). However, the ratio was much less than values reported for regions in India (Dickerson et al.,

ACPD
11, 4447–4485, 2011

2002), which implies that the type of burning mass has a substantial effect on BC emissions. In studies of urban plumes, observations of the ΔBC/ΔCO ratio have not always agreed well from region to region owing to the diverse mixture of emission sources. In these case studies, the ΔBC/ΔCO ratio of urban plumes in Eastern China was $5.3 \pm 0.53\,\mathrm{ng\,m^{-3}\,ppbv^{-1}}$, which is approximately same with the results (ΔBC/ΔCO ratio of $5.7 \pm 0.14\,\mathrm{ng\,m^{-3}\,ppbv^{-1}}$) reported by Kondo et al. for Tokyo (Kondo et al., 2006). Their studies emphasized the temperature dependence of BC and CO emissions from vehicles engines, and studies performed in Beijing supported the argument that CO emissions increased during the warming-up of a vehicle under cold conditions when the temperature of the catalyst is not sufficiently high, and the ΔBC/ΔCO ratio was 3.5–$5.8\,\mathrm{ng\,m^{-3}\,ppbv^{-1}}$ in winter and autumn (Han et al., 2009). Herein, the lower temperature could be a possible explanation of the low ΔBC/ΔCO ratio, and coal and biofuel combustion for domestic heating could account for the increase in the CO atmospheric concentration. Recent studies in Taiwan reported a spatially averaged ΔBC/ΔCO value of $5.3\,\mathrm{ng\,m^{-3}\,ppbv^{-1}}$, which is a typical ratio of ΔBC/ΔCO on a regional scale (Chou et al., 2010). McMeeking et al. pointed out that the ΔBC/ΔCO ratio in Europe urban plumes ranged from 0.8 to $6.2\,\mathrm{ng\,m^{-3}\,ppbv^{-1}}$, and the highest ΔBC/ΔCO ratio was observed for the areas classified as far-outflow and background (ratio of $O_3/NO_x > 10$), where air masses were more chemically processed. This attribution highlights the importance of emission sources over BC or CO processing and removal mechanisms (McMeeking et al., 2010). Owing to such large observed variations and uncertainties concerning the photochemical processing, care should be taken when implementing evaluating emission inventories, and more comprehensive analyses of carbonaceous chemical and physical properties are urgently needed.

9 Conclusions

The BC mass concentration and CO mixing ratio were measured at the summit of Mt Huangshan from June 2006 to May 2009 to investigate the BC–CO relationship

ACPD
11, 4447–4485, 2011

of urban plumes from different regions in Eastern China. The ΔBC/ΔCO ratio is an essential restraint in improving the BC emission inventory and further modeling calculations of regional/global climate forcing. The seasonal variation in the BC concentration had a bimodal distribution with a minimum in summer and two peaks in May and October, when there was large-scale burning of crop residues. The CO concentration increased sharply in the winter "heating period" in Northern China, and the yearly averaged BC and CO concentrations were $654.6 \pm 633.4\,\mathrm{ng\,m^{-3}}$ and 424.1 ± 159.2 ppbv, respectively. Over the whole observation period, BC and CO concentrations and the ΔBC/ΔCO ratio had unimodal diurnal variations, with maxima during the day (09:00–17:00 LST) and minima at night (21:00–04:00 LST) owing to the uplift of pollution with the transport of valley breeze and PBL development during the day and intrusions of clean air from the upper troposphere at night. Cluster analysis using data for which the ambient RH was less than 50% for the whole 48 h back trajectory indicated that the ΔBC/ΔCO ratios of plumes from Central Eastern, Northern, Yangtze River Delta and southern regions of China were 5.65 ± 0.58, 5.2 ± 0.63, 6.58 ± 0.96 and 5.21 ± 0.93 ng/m3/ppbv, respectively. Six episodes of heavy BC pollution (with daily mean BC concentrations exceeding $1000\,\mathrm{ng\,m^{-3}}$) were investigated at the observation site. Results showed that the ΔBC/ΔCO ratio for urban plumes was $5.0–5.7\,\mathrm{ng\,m^{-3}\,ppbv^{-1}}$, which is similar to ratios obtained from an emission inventory, and the BC–CO relation and atmospheric BC and CO loadings in urban areas seemed to be mainly attributed to transportation and industry. The ΔBC/ΔCO ratio was $12.4 \pm 1.5\,\mathrm{ng\,m^{-3}\,ppbv^{-1}}$ during periods influenced by the burning of biomass. Additionally, the loss of BC (removal efficiency of BC due to wet removal in aging processes) during transportation was also estimated on the basis of the ΔBC/ΔCO–RH relationship along air mass pathways. Results show that 30–50% of BC was lost when air mass traveled under higher RH conditions (RH > 60%) for 2 days and over 90% of BC was lost when pollution air masses remained for more than 48 h in an environment with RH exceeding 80%. Furthermore, the BC loss rate of air masses from Southeastern China was about three times that of air masses from Northern China, which highlighted

ACPD
11, 4447–4485, 2011

the importance of the chemical composition of the BC coating and the size distribution of aerosol particles.

Supplementary material related to this article is available online at: http://www.atmos-chem-phys-discuss.net/11/4447/2011/acpd-11-4447-2011-supplement.pdf.

Acknowledgements. The authors would like to thank all staff of the meteorological station at Mt Huangshan for providing lots of conveniences in daily instrument maintenance and data requisition during the observations. We gratefully acknowledge the anonymous reviewers and many Japanese researchers Hitoshi Irie, Masayuki Takigawa, Hisahiro Takashima, Fumikazu Taketani at the JAMSTEC for their helpful comments and suggestions. This work is supported by National Basic Research 973 project (2010CB4951804) and NSFC grant (40775077) and the Global Environment Research Fund (S-7, C-081, B-051) by the Ministry of the Environment, Japan.

References

Adachi, K., Chung, S., and Buseck, P.: Shapes of soot aerosol particles and implications for their effects on climate, J. Geophys. Res., 115(D15), D15206, doi:10.1029/2009JD012868, 2010.

Babu, S. S., Satheesh, S. K., and Moorthy, K. K.: Aerosol radiative forcing due to enhanced black carbon at an urban site in India, Geophys. Res. Lett., 29(18), 1880, doi:10.1029/2002GL015826, 2002.

Badarinath, K. V. S. and Latha, K. M.: Direct radiative forcing from black carbon aerosols over urban environment, Adv. Space Res., 37(12), 2183–2188, 2006.

Badarinath, K. V. S., Kharol, S. K., Chand, T. R. K., Parvathi, Y. G., Anasuya, T., and Jyothsna, A. N.: Variations in black carbon aerosol, carbon monoxide and ozone over an urban area of Hyderabad, India, during the forest fire season, Atmos. Res., 85(1), 18–26, 2007.

Baumgardner, D., Raga, G., Peralta, O., Rosas, I., Castro, T., Kuhlbusch, T., John, A., and Pet-

ACPD

11, 4447–4485, 2011

zold, A.: Diagnosing black carbon trends in large urban areas using carbon monoxide measurements, J. Geophys. Res.-Atmos., 107(D21), 8342, doi:10.1029/2001JD000626, 2002.
Bond, T. C., Streets, D. G., Yarber, K. F., Nelson, S. M., Woo, J.-H., and Klimont, Z.: A technology-based global inventory of black and organic carbon emissions from combustion, J. Geophys. Res., 109(D14), D14203, doi:10.1029/2003JD003697, 2004.
Cao, G. L., Zhang, X. Y., and Zheng, F. C.: Inventory of black carbon and organic carbon emissions from China, Atmos. Environ., 40(34), 6516–6527, 2006.
Cao, J. J., Lee, S. C., Chow, J. C., Watson, J. G., Ho, K. F., Zhang, R. J., Jin, Z. D., Shen, Z. X., Chen, G. C., Kang, Y. M., Zou, S. C., Zhang, L. Z., Qi, S. H., Dai, M. H., Cheng, Y., and Hu, K.: Spatial and seasonal distributions of carbonaceous aerosols over China, J. Geophys. Res., 112(D22), D22S11, doi:10.1029/2006JD008205, 2007.
Cao, J. J., Zhu, C. S., Chow, J. C., Watson, J. G., Han, Y. M., Wang, G. H., Shen, Z. X., and An, Z. S.: Black carbon relationships with emissions and meteorology in Xi'an, China, Atmos. Res., 94(2), 194–202, 2009.
Chen, Y. J., Zhi, G. R., Feng, Y. L., Liu, D. Y., Zhang, G., Li, J., Sheng, G. Y., and Fu, J. M.: Measurements of black and organic carbon emission factors for household coal combustion in China: implication for emission reduction, Environ. Sci. Technol., 43(24), 9495–9500, 2009.
Chou, C. C.-K., Lee, C. T., Cheng, M. T., Yuan, C. S., Chen, S. J., Wu, Y. L., Hsu, W. C., Lung, S. C., Hsu, S. C., Lin, C. Y., and Liu, S. C.: Seasonal variation and spatial distribution of carbonaceous aerosols in Taiwan, Atmos. Chem. Phys., 10, 9563–9578, doi:10.5194/acp-10-9563-2010, 2010.
Chow, J. C., Watson, J. G., Doraiswamy, P., Chen, L. W. A., Sodeman, D. A., Lowenthal, D. H., Park, K., Arnott, W. P., and Motallebi, N.: Aerosol light absorption, black carbon, and elemental carbon at the Fresno Supersite, California, Atmos. Res., 93(4), 874–887, 2009.
Chung, S. H. and Seinfeld, J. H.: Climate response of direct radiative forcing of anthropogenic black carbon, J. Geophys. Res.-Atmos., 110(D11), 22, 25 pp., doi:10.1029/2004JD005441, 2005.
Conant, W. C., Nenes, A., and Seinfeld, J. H.: Black carbon radiative heating effects on cloud microphysics and implications for the aerosol indirect effect – 1. Extended Kohler theory, J. Geophys. Res.-Atmos., 107(D21), 9 pp., doi:10.1029/2002JD002094, 2002.
Cooke, W. F. and Wilson, J. J. N.: A global black carbon aerosol model, J. Geophys. Res., 101(D14), 19395–19409, 1996.
Cozic, J., Mertes, S., Verheggen, B., Cziczo, D. J., Gallavardin, S. J., Walter, S., Bal-

ACPD
11, 4447–4485, 2011

tensperger, U., and Weingartner, E.: Black carbon enrichment in atmospheric ice particle residuals observed in lower tropospheric mixed phase clouds, J. Geophys. Res.-Atmos., 113(D15), 11 pp., doi:10.1029/2007JD009266, 2008.
Croft, B., Lohmann, U., and von Salzen, K.: Black carbon ageing in the Canadian Centre for Climate modelling and analysis atmospheric general circulation model, Atmos. Chem. Phys., 5, 1931–1949, doi:10.5194/acp-5-1931-2005, 2005.
Derwent, R. G., Ryall, D. B., Jennings, S. G., Spain, T. G., and Simmonds, P. G.: Black carbon aerosol and carbon monoxide in European regionally polluted air masses at Mace Head, Ireland during 1995–1998, Atmos. Environ., 35(36), 6371–6378, 2001.
Dickerson, R. R., Andreae, M. O., Campos, T., Mayol-Bracero, O. L., Neusuess, C., and Streets, D. G.: Analysis of black carbon and carbon monoxide observed over the Indian Ocean: implications for emissions and photochemistry, J. Geophys. Res.-Atmos., 107(D19), 8017, doi:10.1029/2001JD000501, 2002.
Han, S., Kondo, Y., Oshima, N., Takegawa, N., Miyazaki, Y., Hu, M., Lin, P., Deng, Z., Zhao, Y., Sugimoto, N., and Wu, Y.: Temporal variations of elemental carbon in Beijing, J. Geophys. Res., 114(D23), D23202, doi:10.1029/2009JD012027, 2009.
Han, Z., Zhang, R., Wang, Q. G., Wang, W., Cao, J., and Xu, J.: Regional modeling of organic aerosols over China in summertime, J. Geophys. Res., 113(D11), D11202, doi:10.1029/2007JD009436, 2008.
Hitzenberger, R., Petzold, A., Bauer, H., Ctyroky, P., Pouresmaeil, P., Laskus, L., and Puxbaum, H.: Intercomparison of thermal and optical measurement methods for elemental carbon and black carbon at an urban location, Environ. Sci. Technol., 40(20), 6377–6383, 2006.
IPCC: Climate change 2001: synthesis report, Cambridege University Press, New York, USA, 2001.
Jacobson, M. Z.: Strong radiative heating due to the mixing state of black carbon in atmospheric aerosols, Nature, 409(6821), 695–697, 2001.
Jennings, S. G., Spain, T. G., Doddridge, B. G., Maring, H., Kelly, B. P., and Hansen, A. D. A.: Concurrent measurements of black carbon aerosol and carbon monoxide at Mace Head, J. Geophys. Res.-Atmos., 101(D14), 19447–19454, 1996.
Kanaya, Y., Komazaki, Y., Pochanart, P., Liu, Y., Akimoto, H., Gao, J., Wang, T., and Wang, Z.: Mass concentrations of black carbon measured by four instruments in the middle of Central East China in June 2006, Atmos. Chem. Phys., 8, 7637–7649, doi:10.5194/acp-8-7637-

ACPD
11, 4447–4485, 2011

2008, 2008.
Kondo, Y., Komazaki, Y., Miyazaki, Y., Moteki, N., Takegawa, N., Kodama, D., Deguchi, S., Nogami, M., Fukuda, M., and Miyakawa, T.: Temporal variations of elemental carbon in Tokyo, J. Geophys. Res., 111, D12205, doi:10.1029/2005JD006257, 2006.
Kondo, Y., Sahu, L., Takegawa, N., Miyazaki, Y., Han, S., Moteki, N., Hu, M., Kim Oanh, N., and Kim, Y.: Stabilization of the mass absorption cross section of black carbon for filter-based absorption photometry by the use of a heated inlet, Aerosol Sci. Tech., 43(8), 741–756, 2009.
Kuwata, M., Kondo, Y., and Takegawa, N.: Critical condensed mass for activation of black carbon as cloud condensation nuclei in Tokyo, J. Geophys. Res.-Atmos., 114(D20202), 9 pp., doi:10.1029/2009JD012086, 2009.
Li, C., Marufu, L. T., Dickerson, R. R., Li, Z., Wen, T., Wang, Y., Wang, P., Chen, H., and Stehr, J. W.: In situ measurements of trace gases and aerosol optical properties at a rural site in Northern China during East Asian study of tropospheric aerosols: an international regional experiment 2005, J. Geophys. Res., 112(D22), D22S04, 16 pp., doi:10.1029/2006JD007592, 2007.
Li, G., Zhang, R., Fan, J., and Tie, X.: Impacts of black carbon aerosol on photolysis and ozone, J. Geophys. Res., 110(D23), D23206, doi:10.1029/2005JD005898, 2005.
Li, J., Wang, Z., Akimoto, H., Yamaji, K., Takigawa, M., Pochanart, P., Liu, Y., Tanimoto, H., and Kanaya, Y.: Near-ground ozone source attributions and outflow in Central Eastern China during MTX2006, Atmos. Chem. Phys., 8, 7335–7351, doi:10.5194/acp-8-7335-2008, 2008.
Liu, X. H., Penner, J. E., and Wang, M. H.: Influence of anthropogenic sulfate and black carbon on upper tropospheric clouds in the NCAR CAM3 model coupled to the IMPACT global aerosol model, J. Geophys. Res.-Atmos., 114, D03204, doi:10.1029/2008JD010492, 2009.
McMeeking, G. R., Hamburger, T., Liu, D., Flynn, M., Morgan, W. T., Northway, M., Highwood, E. J., Krejci, R., Allan, J. D., Minikin, A., and Coe, H.: Black carbon measurements in the boundary layer over western and northern Europe, Atmos. Chem. Phys., 10, 9393–9414, doi:10.5194/acp-10-9393-2010, 2010.
Ming, J., Cachier, H., Xiao, C., Qin, D., Kang, S., Hou, S., and Xu, J.: Black carbon record based on a shallow Himalayan ice core and its climatic implications, Atmos. Chem. Phys., 8, 1343–1352, doi:10.5194/acp-8-1343-2008, 2008.
Ming, J., Xiao, C. D., Cachier, H., Qin, D. H., Qin, X., Li, Z. Q., and Pu, J. C.: Black Carbon (BC) in the snow of glaciers in West China and its potential effects on albedos, Atmos. Res.,

ACPD
11, 4447–4485, 2011

92(1), 114–123, 2009.
Naoe, H., Hasegawa, S., Heintzenberg, J., Okada, K., Uchiyama, A., Zaizen, Y., Kobayashi, E., and Yamazaki, A.: State of mixture of atmospheric submicrometer black carbon particles and its effect on particulate light absorption, Atmos. Environ., 43(6), 1296–1301, 2009.
Nenes, A., Conant, W. C., and Seinfeld, J. H.: Black carbon radiative heating effects on cloud microphysics and implications for the aerosol indirect effect – 2. cloud microphysics, J. Geophys. Res.-Atmos., 107(D21), 11 pp., doi:10.1029/2002JD002101, 2002.
Oberdörster, G. and Yu, C.: The carcinogenic potential of inhaled diesel exhaust: a particle effect?, J. Aerosol Sci., 21, S397–S401, 1990.
Ohara, T., Akimoto, H., Kurokawa, J., Horii, N., Yamaji, K., Yan, X., and Hayasaka, T.: An Asian emission inventory of anthropogenic emission sources for the period 1980–2020, Atmos. Chem. Phys., 7, 4419–4444, doi:10.5194/acp-7-4419-2007, 2007.
Pan, X. L., Yan, P., Tang, J., Ma, J. Z., Wang, Z. F., Gbaguidi, A., and Sun, Y. L.: Observational study of influence of aerosol hygroscopic growth on scattering coefficient over rural area near Beijing mega-city, Atmos. Chem. Phys., 9, 7519–7530, doi:10.5194/acp-9-7519-2009, 2009.
Petzold, A., Schloesser, H., Sheridan, P. J., Arnott, W. P., Ogren, J. A., and Virkkula, A.: Evaluation of multiangle absorption photometry for measuring aerosol light absorption, Aerosol Sci. Tech., 39(1), 40–51, 2005.
Qu, W. J., Arimoto, R., Zhang, X. Y., Zhao, C. H., Wang, Y. Q., Sheng, L. F., and Fu, G.: Spatial distribution and interannual variation of surface PM_{10} concentrations over eighty-six Chinese cities, Atmos. Chem. Phys., 10, 5641–5662, doi:10.5194/acp-10-5641-2010, 2010.
Ramana, M. V., Ramanathan, V., Feng, Y., Yoon, S. C., Kim, S. W., Carmichael, G. R., and Schauer, J. J.: Warming influenced by the ratio of black carbon to sulphate and the black-carbon source, Nat. Geosci., 3(8), 542–545, 2010.
Ramanathan, V.: Role of Black Carbon in Global and Regional Climate Changes, House Committee on Oversight and Government Reform, Washington DC, 17 pp., 2007.
Ramanathan, V. and Carmichael, G.: Global and regional climate changes due to black carbon, Nat. Geosci., 1(4), 221–227, 2008.
Reisinger, P., Wonaschutz, A., Hitzenberger, R., Petzold, A., Bauer, H., Jankowski, N., Puxbaum, H., Chi, X., and Maenhaut, W.: Intercomparison of measurement techniques for black or elemental carbon under urban background conditions in wintertime: influence of biomass combustion, Environ. Sci. Technol., 42(3), 884–889, 2008.
Sato, M., Hansen, J., Koch, D., Lacis, A., Ruedy, R., Dubovik, O., Holben, B., Chin, M., and

ACPD
11, 4447–4485, 2011

Novakov, T.: Global atmospheric black carbon inferred from AERONET, P. Natl. Acad. Sci. USA, 100(11), 6319, 2003.
Schwarz, J. P., Spackman, J. R., Fahey, D. W., Gao, R. S., Lohmann, U., Stier, P., Watts, L. A., Thomson, D. S., Lack, D. A., Pfister, L., Mahoney, M. J., Baumgardner, D., Wilson, J. C., and Reeves, J. M. : Coatings and their enhancement of black carbon light absorption in the tropical atmosphere, J. Geophys. Res.-Atmos., 113(D3), doi:10.1029/2007JD009042, 2008.
Seinfeld, J.: Atmospheric science – black carbon and brown clouds, Nat. Geosci., 1(1), 15–16, 2008.
Slowik, J. G., Cross, E. S., Han, J., Davidovits, P., Onasch, T. B., Jayne, J. T., Williams, L. R., Canagaratna, M. R., Worsnop, D. R., Chakrabarty, R. K., Moosmüller, H., Arnott, W. P., Schwarz, J. P., Gao, R. S., Fahey, D. W., Kok, G. L., and Petzold, A.: An inter-comparison of instruments measuring black carbon content of soot particles, Aerosol Sci. Tech., 41(3), 295–314, 2007.
Spackman, J. R., Schwarz, J. P., Gao, R. S., Watts, L. A., Thomson, D. S., Fahey, D. W., Holloway, J. S., de Gouw, J. A., Trainer, M., and Ryerson, T. B.: Empirical correlations between black carbon aerosol and carbon monoxide in the lower and middle troposphere, Geophys. Res. Lett., 35(19), L19816, doi:10.1029/2008GL035237, 2008.
Streets, D. G. and Aunan, K.: The importance of China's household sector for black carbon emissions, Geophys. Res. Lett., 32(12), doi:10.1029/2005GL022960, 2005.
Streets, D. G., Gupta, S., Waldhoff, S. T., Wang, M. Q., Bond, T. C., and Bo, Y. Y.: Black carbon emissions in China, Atmos. Environ., 35(25), 4281–4296, 2001.
Streets, D., Yarber, K., Woo, J., and Carmichael, G.: Biomass burning in Asia: annual and seasonal estimates and atmospheric emissions, Global Biogeochem. Cy., 17(4), doi:10.1029/2005GL022960, 2003a.
Streets, D., Bond, T., Carmichael, G., Fernandes, S., Fu, Q., He, D., Klimont, Z., Nelson, S., Tsai, N., and Wang, M.: An inventory of gaseous and primary aerosol emissions in Asia in the year 2000, J. Geophys. Res., 108(D21), 8809, 2003b.
Subramanian, R., Kok, G. L., Baumgardner, D., Clarke, A., Shinozuka, Y., Campos, T. L., Heizer, C. G., Stephens, B. B., de Foy, B., Voss, P. B., and Zaveri, R. A.: Black carbon over Mexico: the effect of atmospheric transport on mixing state, mass absorption cross-section, and BC/CO ratios, Atmos. Chem. Phys., 10, 219–237, doi:10.5194/acp-10-219-2010, 2010.
Thevenon, F., Anselmetti, F. S., Bernasconi, S. M., and Schwikowski, M.: Mineral dust and elemental black carbon records from an Alpine ice core (Colle Gnifetti glacier) over the last

ACPD
11, 4447–4485, 2011

millennium, J. Geophys. Res.-Atmos., 114(D17102), 11 pp., doi:10.1029/2008JD011490, 2009.

Uno, I., Carmichael, G. R., Streets, D., Satake, S., Takemura, T., Woo, J. H., Uematsu, M., and Ohta, S.: Analysis of surface black carbon distributions during ACE-Asia using a regional-scale aerosol model, J. Geophys. Res.-Atmos., 108(D23), 8636, doi:10.1029/2002JD003252, 2003.

Wang, Z., Li, J., Wang, X., Pochanart, P., and Akimoto, H.: Modeling of regional high ozone episode observed at two mountain sites (Mt. Tai and Huang) in East China, J. Atmos. Chem., 55(3), 253–272, 2006.

Yamaji, K., Li, J., Uno, I., Kanaya, Y., Irie, H., Takigawa, M., Komazaki, Y., Pochanart, P., Liu, Y., Tanimoto, H., Ohara, T., Yan, X., Wang, Z., and Akimoto, H.: Impact of open crop residual burning on air quality over Central Eastern China during the Mount Tai Experiment 2006 (MTX2006), Atmos. Chem. Phys., 10, 7353–7368, doi:10.5194/acp-10-7353-2010, 2010.

Yan, P., Tang, J., Huang, J., Mao, J. T., Zhou, X.J., Liu, Q., Wang, Z. F., and Zhou, H. G.: The measurement of aerosol optical properties at a rural site in Northern China, Atmos. Chem. Phys., 8, 2229–2242, doi:10.5194/acp-8-2229-2008, 2008.

Yan, X., Ohara, T., and Akimoto, H.: Bottom-up estimate of biomass burning in mainland China, Atmos. Environ., 40(27), 5262–5273, 2006.

Zhang, Q., Streets, D. G., Carmichael, G. R., He, K. B., Huo, H., Kannari, A., Klimont, Z., Park, I. S., Reddy, S., Fu, J. S., Chen, D., Duan, L., Lei, Y., Wang, L. T., and Yao, Z. L.: Asian emissions in 2006 for the NASA INTEX-B mission, Atmos. Chem. Phys., 9, 5131–5153, doi:10.5194/acp-9-5131-2009, 2009.

Zhang, R.-J., Cao, J.-J., Lee, S.-C., Shen, Z.-X., and Ho, K.-F.: Carbonaceous aerosols in PM_{10} and pollution gases in winter in Beijing, J. Environ. Sci., 19(5), 564–571, 2007.

ACPD
11, 4447–4485, 2011

Table 1. Statistical results of BC and CO concentrations and BC–CO correlations for each cluster.

Cluster category	BC ($ng\,m^{-3}$)		CO (ppbv)		$\Delta BC/\Delta CO$[a] ($ng\,m^{-3}\,ppbv^{-1}$)	Intercepts (ppbv)	R[b]	N[c]
	Mean	S.D.	Mean	S.D.				
#1	750.9	616.7	319.5	94.7	5.65±0.58	187.1±17.1	0.86	16 800
#2	801.3	632.6	356.3	113.1	5.20±0.63	195.2±24.3	0.87	11 160
#3	422.4	487.8	244.9	73.2	6.58±0.96	178.0±14.4	0.98	1320
#4	942.4	612.8	366.4	111.8	5.21±0.93	186.8±38.7	0.94	2280

[a] Values are written as mean ± 3σ.
[b] At the 95% significance level.
[c] Number of one-minute averaged data.

ACPD
11, 4447–4485, 2011

Table 2. The ΔBC/ΔCO ratio in episodes of heavy BC pollution and comparison with results of other studies.

Episode	Date	Mean CO (ppbv)	CO Max.	Mean BC ($ng\,m^{-3}$)	BC Max.	ΔBC/ΔCO ($ng\,m^{-3}$/ppb)	Hotspots[a] (N)	Types
1	29–31 Jan 2007	429.6	622.4	1285.6	2892.9	5.3±0.10	3	urban plume
2	6 Feb 2007	515.0	623.3	1797.5	2821.4	5.0±0.18	20	urban plume
3	28 Oct 2007	325.2	532.6	1071.2	2678.6	5.8±0.36	0	urban plume
4	29 Oct 2007	743.8	887.0	1065.8	2714.3	5.0±0.81	2	urban plume
5	22–24 Oct 2007	457.3	590.5	2452.2	5050.0	12.4±1.5	35	BB
6	6–8 Jan 2008	583.7	843.7	2294.7	4185.7	7.5±0.18	812	BB+ urban

[a] Statistical results possibly underestimate the total number of hotspots because some fire points were likely blocked by clouds.
[b] BB represents biomass burning.

ACPD
11, 4447–4485, 2011

Table 3. Relationship between the ΔBC/ΔCO ratio and RH for all data.

RH[a] (%) Range	Mean	Std.	ΔBC/ΔCO ($ng\,m^{-3}\,ppbv^{-1}$) Mean	Std.	N[b]
> 80	91.6	5.0	0.4	0.4	148
65–85	74.4	4.3	1.0	0.6	157
55–75	61.4	4.7	1.6	0.7	113
45–65	56.6	4.4	2.2	0.7	110
35–55	43.4	4.4	3.2	0.7	115
< 40	29.3	19.7	5.3	0.3	467

[a] RH is the mean value for episodes when meteorology along air mass pathways met the required RH condition.
[b] Number of hourly averaged data points.

ACPD
11, 4447–4485, 2011

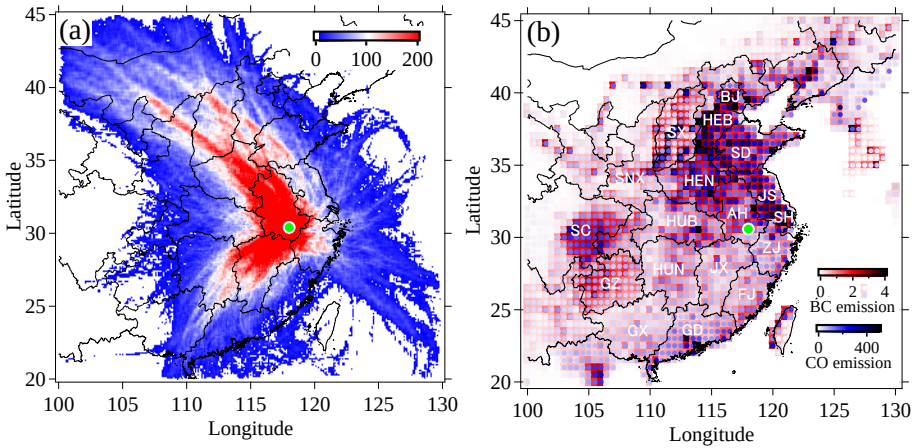

Fig. 1. Spatial distributions of air mass back trajectories and BC and CO emissions in 2006. The green dots indicate the location of the observation site. **(a)** The 48 h air mass pathways were computed for the period 2006–2009 using the NECP/GDAS1 database with a starting point altitude of 1500 m. Red indicates more than 100 instances of air masses passing through the ($0.01^\circ \times 0.01^\circ$) grid, whereas occurrences of less than 10 times are neglected. **(b)** Total anthropogenic (industrial, residential, transportation, and power) emissions of BC and CO are presented in units of Gg yr^{-1} ($0.5^\circ \times 0.5^\circ$) grid^{-1}. The red square and blue dot in each grid represent the BC and CO emissions, respectively; a darker color indicates stronger emission. Abbreviations in the plot are BJ (Beijing), HEB (Hebei), SX (Shanxi), SD (Shandong), HEN (Henan), JS (Jiangsu), SNX (Shaanxi), HUB (Hubei), SC (Sichuan), SH (Shanghai), AH (Anhui), HUN (Hunan), JX (Jiangxi), ZJ (Zhejiang), FJ (Fujian), GD (Guangdong), GX (Guangxi), and GZ (Guizhou).

ACPD
11, 4447–4485, 2011

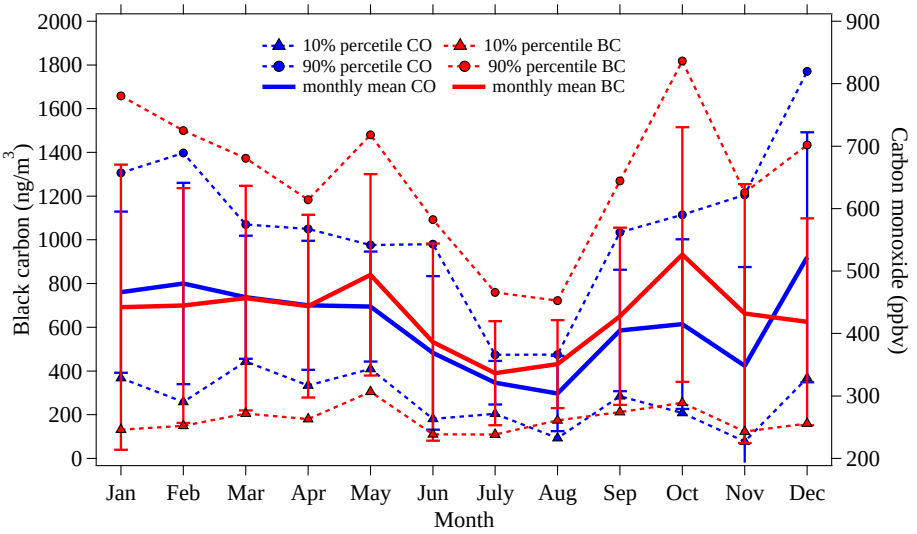

Fig. 2. Seasonal variations in BC (red) and CO (blue) concentrations during the observation period. Circles and triangles represent 90% and 10% percentiles of hourly averaged BC and CO concentrations, respectively. Error bars are also plotted in the figure to indicate monthly variations. In general, BC and CO seasonal variations correlated well owing to their common sources (i.e., biofuel incomplete-combustion processes in industry and transportation) in spite of their different removal mechanisms.

ACPD
11, 4447–4485, 2011

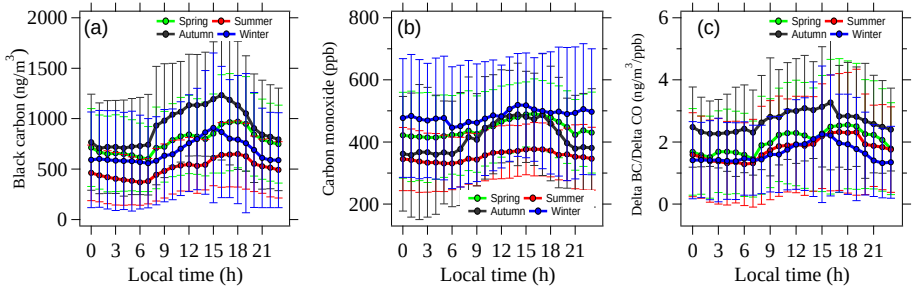

Fig. 3. Diurnal variations in BC, CO and ΔBC/ΔCO for each season. The seasonality in the Mt Huangshan area is distinctive with there being a short spring and autumn. In the plot, spring comprises April and May; summer comprises June, July, August and September; autumn comprises October and November; and winter comprises December, January, February and March.

ACPD
11, 4447–4485, 2011

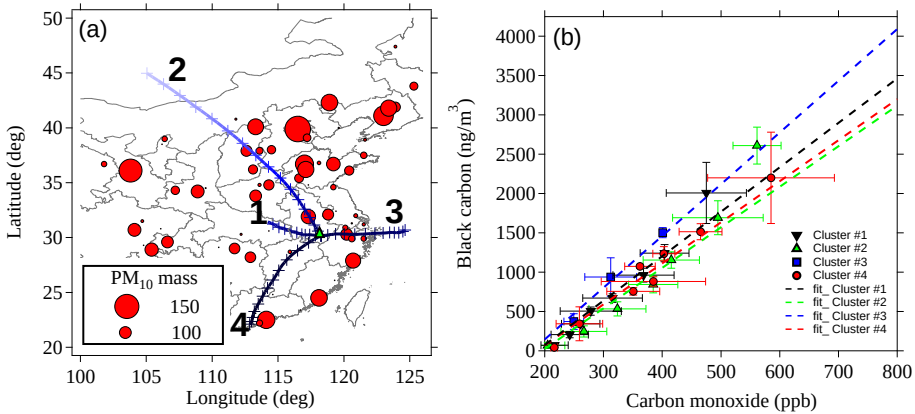

Fig. 4. Classification of 48 h back trajectory air mass pathways and a scatter plot of the BC–CO correlation for each cluster. **(a)** Records from Wuhu (31.3° N, 118.4° E) were excluded owing to suspicious strong daily variations that might be due to strong local emission sources. The size of a filled circle represents the yearly averaged PM_{10} mass concentration. **(b)** Correlation of BC–CO for each cluster. For clarity, data points shown in the figure are 6–8 bin-averaged (original data are shown in supplementary Fig. 1); dashed lines are the linear regression results for each cluster.

ACPD
11, 4447–4485, 2011

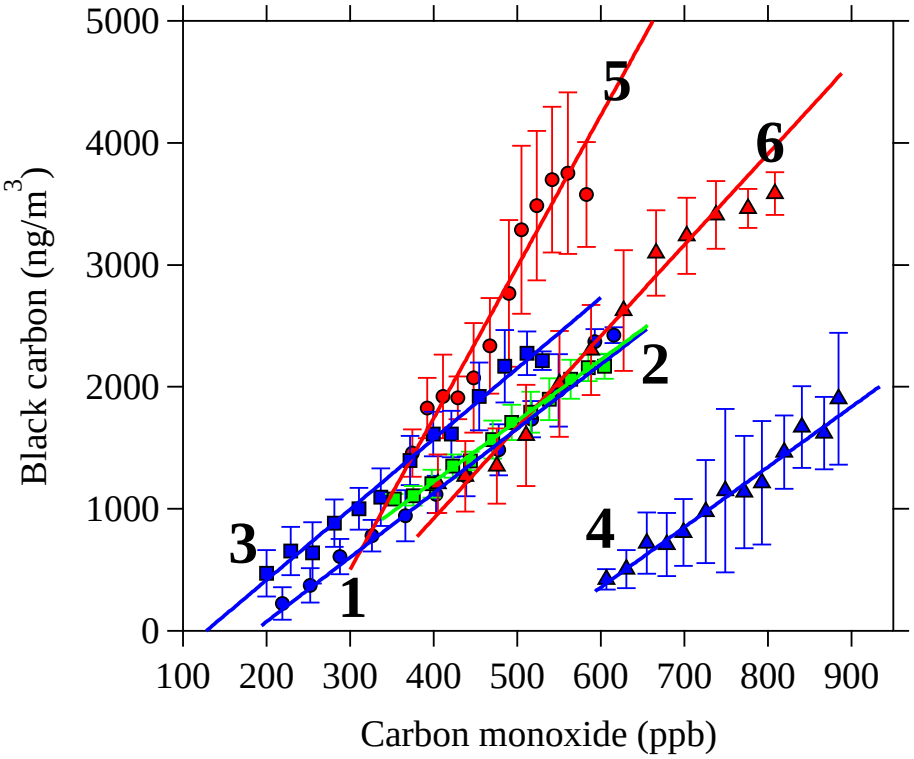

Fig. 5. Scatterplot and linear regression results of the BC–CO correlation during episodes of heavy pollution. All scatterpoints were bin-averaged (individual data are shown in supplementary Figs. 4 and 5), blue and green marks represent episodes of urban plumes, and red marks indicate events of open burning of biomass along air mass pathways. Detailed information is summarized in Table 2.

ACPD
11, 4447–4485, 2011

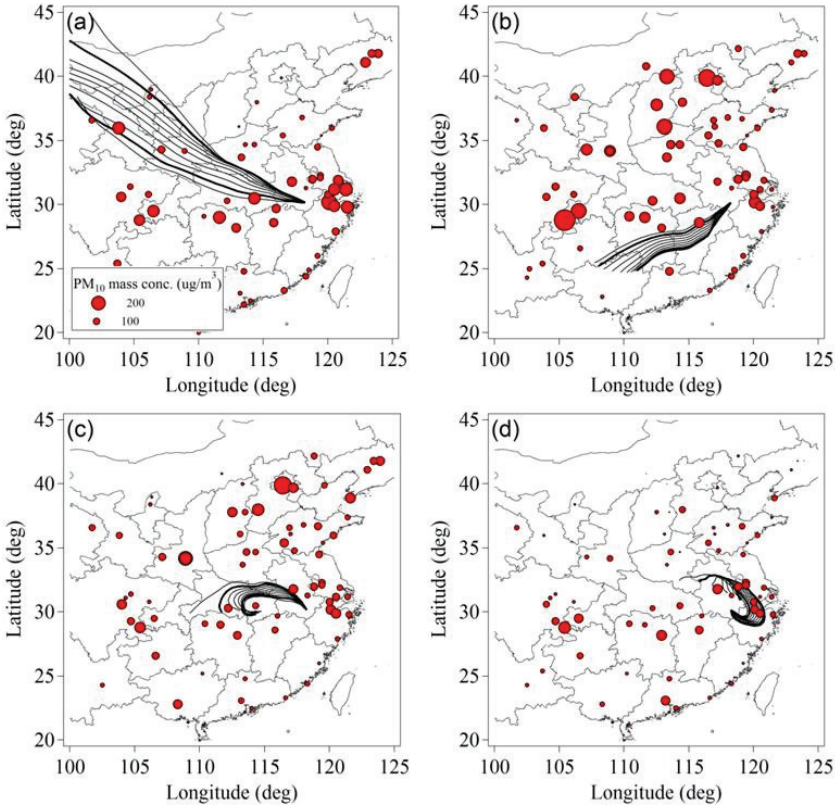

Fig. 6. Forty-eight hour back trajectories of air masses in the cases of urban plume episodes. Back trajectories were plotted at time interval of 2 h and red dots represent daily averaged PM_{10} mass concentrations exceeding 100 ug/m^3 for 85 Chinese cites **(a)** 29 January 2007; **(b)** 6 February 2007; **(c)** 28 October 2007; **(d)** 29 October 2007. To clearly illustrate the spatial distributions of pollution, linear interpolated results are also presented.

ACPD
11, 4447–4485, 2011

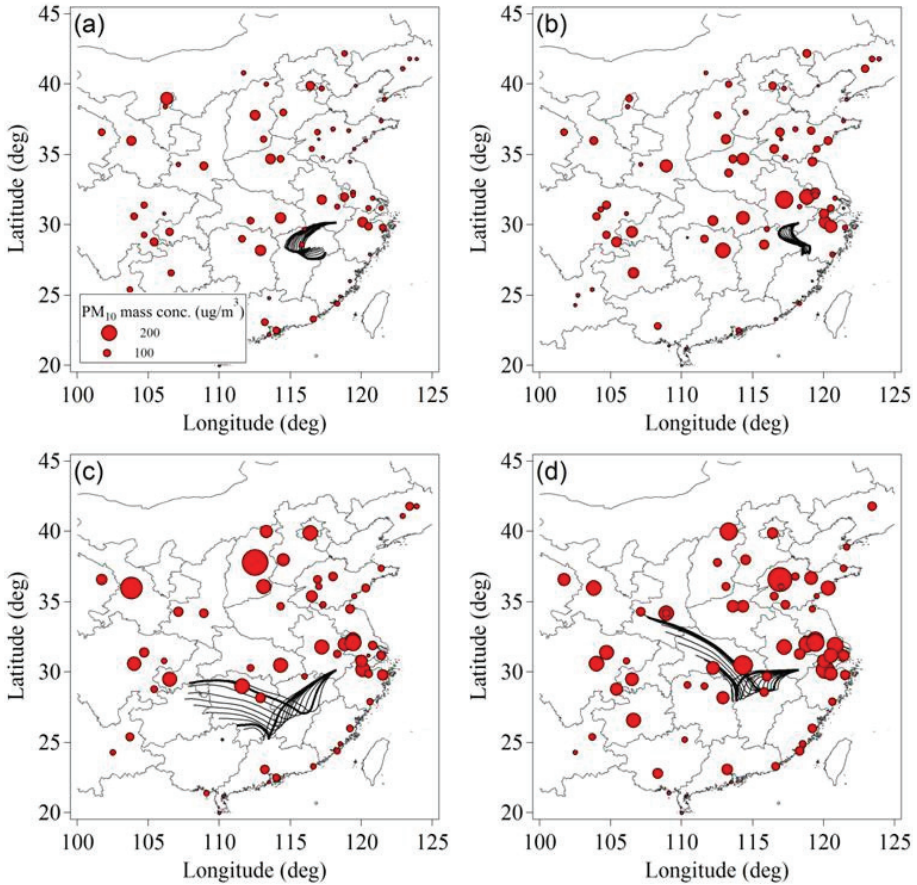

Fig. 7. Forty-eight hour back trajectories of air masses during open-burning events. **(a)** 22 October 2007; **(b)** 24 October 2007; **(c)** 6 January 2008; **(d)** 8 January 2008.

ACPD
11, 4447–4485, 2011

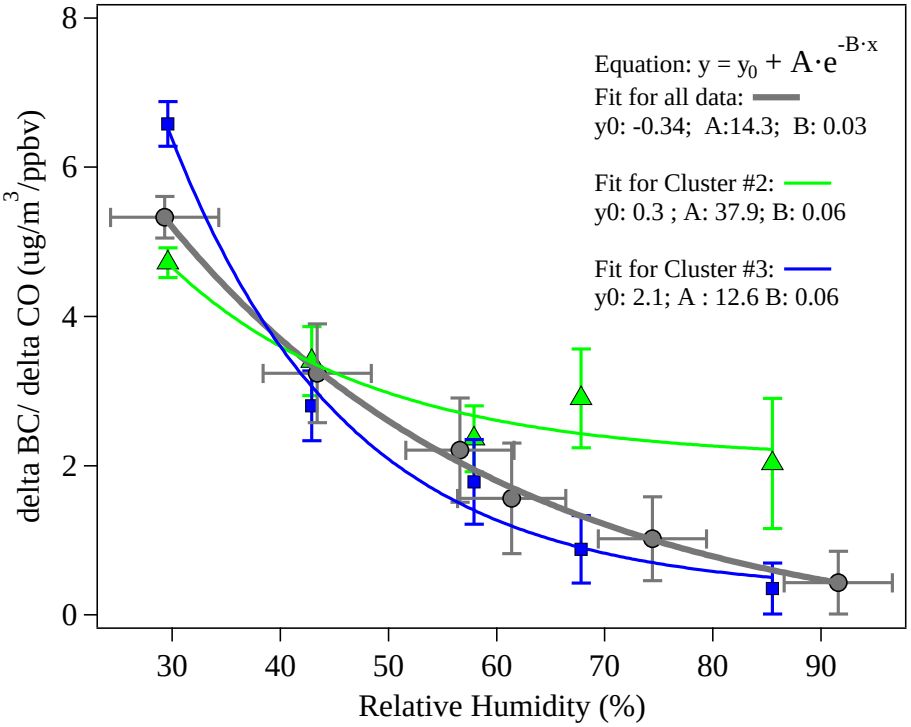

Fig. 8. Dependence of the observed ΔBC/ΔCO ratio on RH at Mt Huangshan for all non-rain periods. Relationship between ΔBC/ΔCO and RH was fitted by exponential function, and the situation for the whole situation is shown by the gray line. The green triangles and blue squares represent for cluster #2 and cluster #3, respectively.

ACPD
11, 4447–4485, 2011